J. Synchrotron Rad. (1997). **4**, 95–101

Laue Orientation Imaging

H. R. Wenk,[a,b,c]† F. Heidelbach,[c,d] D. Chateigner[a] and F. Zontone[d]

[a]Laboratoire de Cristallographie, CNRS, Grenoble, France, [b]Department of Geology and Geophysics, University of California, Berkeley, USA, [c]Center for Materials Science, Los Alamos National Laboratory, Los Alamos, New Mexico, USA, and [d]European Synchrotron Radiation Facility, Grenoble, France. E-mail: wenk@seismo.berkeley.edu

(*Received 10 June 1996; accepted 15 November 1996*)

Advantage was taken of the highly focused X-ray beam (10–30 μm) and the broad white spectrum of synchrotron X-rays at the ESRF for automatic recording of Laue patterns from polycrystals and extraction of orientation information. The procedure used is similar to that applied for electron-backscattering patterns in the scanning electron microscope and provides data for local orientation mapping used in texture analysis. Laue patterns are obtained from a thin slice of material in transmission and recorded with a CCD detector. The Laue geometry is converted into a gnomonic projection in which co-zonal reflections lie on straight lines. On applying the Hough transform these lines are merged into a single point, which is recognized by the computer and assigned zone indices [*uvw*] by comparison with a table of interzonal angles. From the angular positions of several [*uvw*] the crystal orientation is calculated. The method is illustrated for the orthorhombic magnesium silicate olivine.

Keywords: Laue patterns; texture analysis; indexing (automatic); orientation determination; olivine; gnomonic projection.

1. Introduction

The study of crystallite orientation distributions in polycrystalline materials has become important in many disciplines. Deformation of metals may produce anisotropy which is expressed in physical properties. In polymers the orientation of crystallites can be highly preferred and the pronounced texture has a strong influence on the mechanical strength of the material. Deformation in the interior of the Earth, *e.g.* convection in the mantle, produces preferred orientation which is expressed in the observed seismic anisotropy. Growth textures in thin films have become new subjects of texture analysis.

Today, texture is mainly measured using diffraction techniques involving either X-rays, electrons or neutrons. Conventional methods can only measure the average texture of the sample (Bunge, 1982; Wassermann & Grewen, 1962; Wenk, 1985). For some applications it is important to determine the local texture; for example, when the interaction of neighboring grains needs to be evaluated. Here, the orientation of individual grains has to be measured in relation to their position in the sample. Geologists in Innsbruck introduced this method over 50 years ago ['Achsen-Verteilungs-Analyse' of Ramsauer (Sander, 1950)], and later, with the availability of computers, the method was quantified by Wenk & Trommsdorff (1965). Individual orientations were measured with a petrographic microscope, which is a very time-consuming task. More recently, electron microscopes have been used to measure orientations, based on diffraction patterns. In particular, electron-backscattering diffraction patterns, obtained with a scanning electron microscope (SEM), have gained importance (Adams, Wright & Kunze, 1993). With this method it is possible to automatically obtain crystal orientation information from areas as small as 1 μm^2.

Electron-backscattering diffraction patterns are produced in a very thin surface layer (<0.2 μm thick) and require a fairly ideal crystal structure. If the structure contains planar defects (stacking faults with stacking disorder) or linear defects (high dislocation densities), patterns are of such poor quality that they cannot be interpreted. Damage can also be produced during sample preparation, particularly mechanical polishing of ceramics (Kunze, Wright, Adams & Dingley, 1993). If samples are non-conductive, surfaces may charge during experiments, which deteriorates the pattern. Coating with a thin carbon film to prevent charging can also be destructive. Application of the electron-backscattering diffraction-pattern technique is therefore limited.

Gottstein (1988) suggested using a fine beam of synchrotron X-rays to measure local orientations. X-rays produce diffraction patterns from finite volumes rather than thin surface layers and are therefore less subject to the limitations discussed above. At the time, the technology was not available for using this technique. There has been renewed interest using the synchrotron to determine crystal orientations, but patterns could not be interpreted using a large 1 mm beam (Stock, Guvenilir, Piotrowski & Rek,

† Address for correspondence: Department of Geology and Geophysics, University of California, Berkeley, CA 94720, USA.

© 1997 International Union of Crystallography
Printed in Great Britain – all rights reserved

1995). Taking advantage of recent progress in synchrotron sources, detection hardware and data-processing methods, we believe that Laue orientation mapping with synchrotron X-rays has become feasible, as we will demonstrate for a sample of the orthorhombic magnesium silicate olivine, on which we previously failed to obtain satisfactory electron-backscattering diffraction patterns.

2. Sample and experimental technique

The sample used for this pilot experiment was a 100 µm-thick slab (about 1 × 2 cm) of an olivine polycrystal. The geological sample is a peridotite xenolith from a 1801 lava flow of the Hulalai volcano in Hawaii, and probably represents material of the upper mantle which was brought to the surface by volcanic processes. The slab was prepared by sawing and then by mechanical abrasion, as is standard for petrographic thin sections. Inspection with a petrographic microscope confirms that olivine is the major phase and indicates a range of grain sizes between 0.5 and 2 mm. The fragile sample was removed from the supporting glass slide and mounted on a metal frame for easier handling.

The experiment was performed at the 'white beam' station (ID9-BL3) of the European Synchrotron Radiation Facility (ESRF). The focused wiggler beam was reduced to about 30 µm in diameter. After beam conditioning the main intensities were contained in the wavelength range 0.25–0.55 Å (Fig. 1). The intensity of the primary beam was attenuated by passing it through a 1 cm-thick block of aluminium. The sample was mounted on a computer-controlled *xy* stage perpendicular to the incident beam and studied in transmission (Fig. 2). The Laue data were collected automatically at *x* and *y* increments of 100 µm, covering about 1 cm^2 of the sample. Diffracted intensities were recorded with a CCD camera with a fluorescent screen at a distance of 13.1 ± 0.2 cm from the sample (Moy, 1994). The detector size was 12.42 × 11.52 cm (100 µm per pixel). Recording times were near 20 ms per diffraction pattern. The data were treated at the ESRF to correct for image distortion using the local program *FIT2D* (Hammersley, Svensson & Thompson, 1994). Corrected data were then transferred to Los Alamos for further analysis, as described in the following section. Over 1000 patterns were obtained. In this report we only use a single pattern to illustrate the method.

For the purpose of orientation determination, only the position of the Laue spots are of interest, not their intensities. Consequently, corrections for absorption resulting from variation in paths and wavelengths for different spots were not carried out.

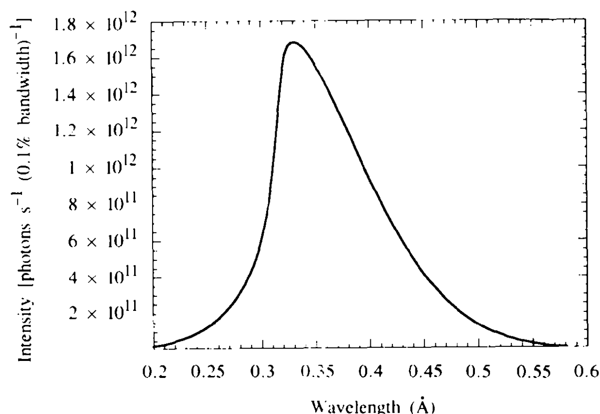

Figure 1
Calculated wavelength spectrum at ID9-BL3; calculation includes absorption from a 1 cm-thick aluminium block.

3. Data processing

Laue patterns were the first recorded diffraction patterns; ever since their discovery, indexing and interpretation has haunted scientists. For monochromatic radiation one can immediately assign a *d*-spacing to a diffraction spot, but for white radiation this is not possible unless one can measure the energy of the diffracted photons with an energy-sensitive detector, *e.g.* for time-of-flight neutron diffraction (Jacobson, 1986). Without an energy-sensitive detector the indexing procedure is far more complicated, but semi-automatic software has been developed enabling users to arrive at good solutions relatively quickly. They are particularly used by protein crystallographers (Helliwell *et al.*, 1989; Laugier & Filhol, 1983; Campbell, Clifton, Harding & Hao, 1995; Greenhough & Shrive, 1994). In these applications, emphasis is on obtaining Laue indices of diffraction spots and the corresponding quantitative intensities, used for structural characterization. All these methods need input and some judgement from the user.

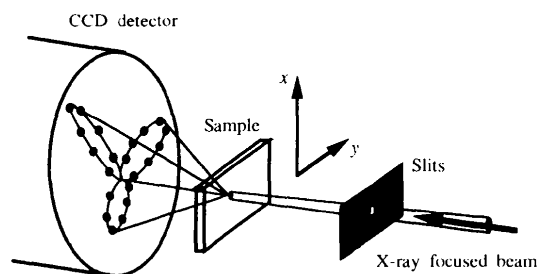

Figure 2
Sketch of experimental setup with source, collimation, *xy* stage and CCD camera.

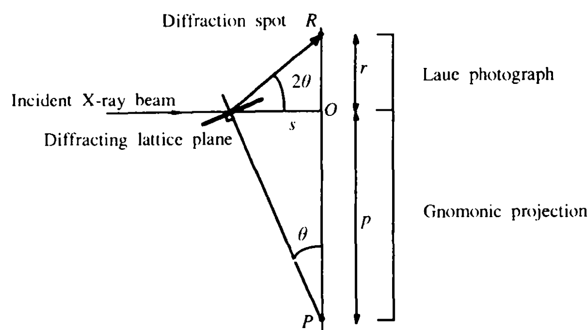

Figure 3
Geometry of the Laue method and the gnomonic projection for reflection on a lattice plane. Symbols are defined in the text.

In our case the situation is different. Similar to the automatic SEM–electron-backscattering diffraction-pattern strategy (Adams *et al.*, 1993), we wish to scan a sample automatically, record thousands of patterns and interpret them in a matter of seconds. The lattice parameters are known, intensities are uninteresting, and all we need are three Euler angles specifying the crystal orientation relative to the sample (*e.g.* Bunge, 1982). For this application the procedure has to be fully automatic.

A Laue pattern can be viewed as a projection of the crystal lattice (Amorós, Buerger & Amorós, 1975). Each lattice plane is represented as a spot R on the film (Fig. 3). Co-zonal lattice planes (having a lattice line in common) have diffracted beams on a cone and, on the detector, lie on a conical section (ellipse, parabola or hyperbola, depending on the Bragg angle, θ). This highly distorted lattice representation can be converted into a more standard crystallographic projection. The gnomonic projection has the advantage that co-zonal lattice planes appear as points which lie on a straight line. The conversion from a Laue pattern to a gnomonic projection is straightforward (Fig. 3):

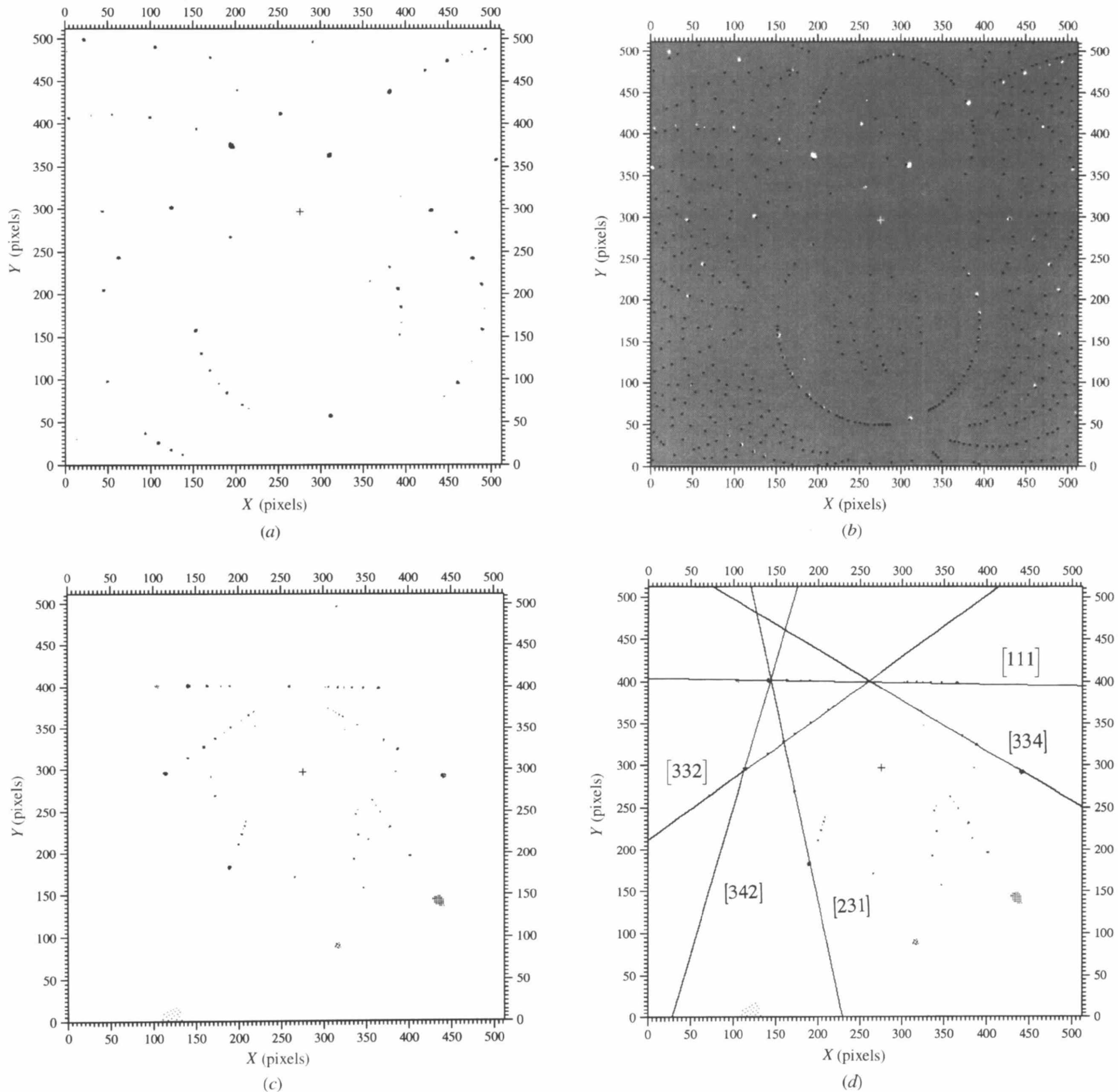

Figure 4
(*a*) Laue pattern of an olivine crystal in an arbitrary orientation; the small cross marks the pattern center; (*b*) the same pattern (white spots) superposed with a theoretical pattern up to $h, k, l < 10$ (black dots) derived from the procedure described in this paper; (*c*) pattern (*a*) transformed into a gnomonic projection; the intensity of all pixels is set to unity; the grid pattern spread over a wide area at the outer edge of the gnomonic projection corresponds to a single reflection close to the origin in the Laue pattern; (*d*) same as (*c*) with zones identified in the analysis of the Hough transform and indexing.

$$p = s \tan (90° - \theta) = s \cot \theta, \quad (1)$$

where p is the distance from the center of the gnomonic projection to the projected point P. The Bragg angle is readily obtained from the distance r of a spot R on the film from the center, if the film is mounted at a distance s from the sample:

$$\theta = 0.5 \arctan (r/s), \quad (2)$$

and hence

$$p = s \cot [0.5 \arctan (r/s)]. \quad (3)$$

Fig. 4(*a*) shows a Laue pattern of olivine in an arbitrary orientation, corrected for instrument distortion and reduced from the original array by binning and cutting to 512 × 512 pixels. Fig. 4(*c*) is the gnomonic projection of the same pattern and intense spots, lying on straight lines, can be recognized. The line is a zone axis and can be used to specify the crystal orientation. The transformation was made for all pixels in Laue space. Because of the distortion, one pixel in Laue space in the central region (low Bragg angles) corresponds to several pixels in gnomonic projection (peripheral region), not all of them having values. This is visible in the grid pattern, *e.g.* in the lower left part of Fig. 4(*c*).

A computer has difficulty in identifying straight lines by the points which define it. Here, the Hough transform, which is also used for electron-backscattering diffraction patterns, is useful (Hough, 1962; Kunze *et al.*, 1993). In the Hough transform each point at coordinates x,y in the gnomonic projection is converted into a sinusoidal curve according to

$$H = x \cos \Phi + y \sin \Phi, \quad (4)$$

where H and Φ are parameters in Hough space (Fig. 5*a*). The curves of all points lying on a straight line (zone) in gnomonic space intersect in one point in Hough space; the coordinates H and Φ of that point define the distance from the origin and the azimuth of the corresponding zone, respectively. The intensity of the Hough curves corresponds to the intensity of pixels in diffraction space. For this analysis it is the number of different reflections contributing to a single Hough maximum that is important, rather than their relative intensity. Therefore, we assigned each pixel in gnomonic projection with an intensity above a certain threshold unit intensity for the Hough transform and the rest of the pattern was assigned zeros. This causes some overemphasis of reflections with low Bragg angles because these spread over more pixels. There was no problem in arriving at the correct solution. In future experiments it may be more elegant to collect all contributions from a reflection in a single pixel in gnomonic space.

In order to smooth the Hough transform for irregularities, and at the same time to sharpen it to emphasize maxima of a certain shape, the Hough transform was processed with a mask of 13 × 13 pixels, which gives the highest weight to the center (Krieger-Lassen, Juul Jensen & Conradsen, 1992). The mask was applied to all 512 × 512 pixels in Hough space for filtering and then the same mask was used to identify the positions of local maxima with the highest intensities, *i.e.* the largest numbers of co-zonal planes (Fig. 5*b*). Each one of these maxima corresponds to a zone with axis [*uvw*]. The maxima in our test case are listed with their Hough parameters (H, Φ) and the standard spherical coordinates (φ, ρ) of their zone axes in Table 1. In Fig. 4(*d*) the position of the identified zones is shown by lines in the gnomonic projection. From spherical coordinates (referred to a Cartesian coordinate system), interaxial angles for all combinations of zone axes identified in the Hough transform were calculated (Table 2).

A similar table was prepared for all possible pairs of lattice directions [*uvw*], with $u, v, w \leq 5$, based on symme-

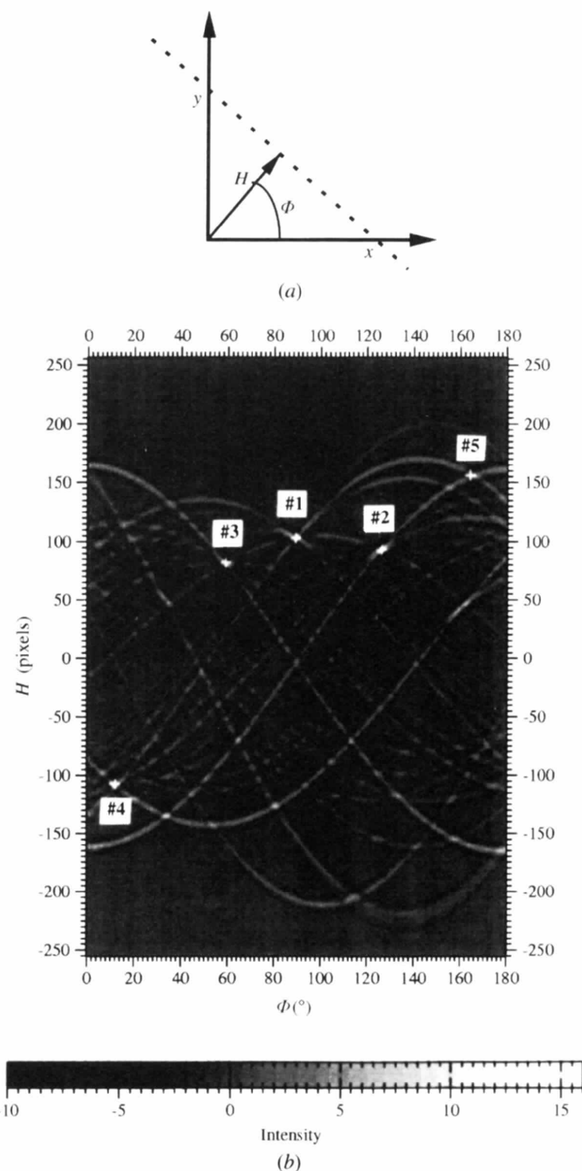

Figure 5
(*a*) Geometry of the Hough transform; (*b*) Hough transform of the gnomonic projection in Fig. 4(*c*) after processing with a filter; the five strongest maxima (zones) are marked with crosses. Numbers refer to Tables 1 and 2.

Table 1
Maxima in Hough space (Φ, H) and corresponding spherical coordinates (φ, ρ) of the zone axes.

#	Intensity (a.u.)	Φ (°)	H (pixel)	φ (°)	ρ (°)
1	23	89	103	269.0	10.3
2	21	126	93	306.0	11.4
3	16	59	82	239.0	12.9
4	14	12	−107	12.0	10.0
5	10	164	156	344.0	6.9

Table 2
Comparison of interaxial angles between pairs of lattice directions identified in the Laue pattern and corresponding angles based on the lattice of an olivine crystal.

Euler angles, which define the orientation of the crystal relative to the sample, were calculated from pairs of indexed lattice directions and their spherical coordinates.

#1	#2	Angle (°)	$[uvw]^1$	$[uvw]^2$	Angle (°)	α (°)	β (°)	γ (°)
1	2	6.9	[111]	[332]	7.0	192.6	70.0	138.9
1	3	6.5	[111]	[334]	6.3	190.8	69.6	138.8
1	4	15.9	[111]	[231]	16.0	192.2	69.9	138.9
1	5	10.8	[111]	[342]	10.9	192.2	69.9	138.9
2	3	13.4	[332]	[334]	13.3	191.7	69.8	139.0
2	4	11.7	[332]	[231]	11.8	192.3	69.9	138.9
2	5	7.3	[332]	[342]	7.5	192.7	70.0	138.9
3	4	21.0	[334]	[231]	21.1	191.5	69.9	139.0
3	5	16.1	[334]	[342]	16.2	191.3	69.9	138.9
4	5	5.0	[231]	[342]	5.0	192.1	70.0	138.8

try and the lattice parameters of olivine (orthorhombic, a = 10.22, b = 5.96, c = 4.81 Å) using the general equation for all crystal symmetries from Barrett & Massalski (1980). This table is very large. The number was reduced by only admitting interaxial angles below 30° that is about the possible range observed on the Laue pattern. The experimental interaxial angles (Table 2, left side) were then compared with the table of calculated angles (Table 2, center). Conditions for acceptance of a match were that the deviation in interaxial angles was less than 1°, the angle was less than 30°, and a choice between symmetrically equivalent directions was made such that all indices of the set and interfacial angles are consistent with a single orientation.

The match between experimental and calculated interaxial angles is reasonably good for all five identified zones, with theoretically derived zones within ±1° for each interaxial angle. The average deviation for all ten interaxial angles is 0.2°. On the basis of this comparison, the computer assigned zone-axis symbols to the unknown zones in the experimental Laue pattern.

Three orthonormal coordinate systems have been defined: one system is the sample, specified by the normal to the planar surface (Z) and a line in that plane (X) (Fig. 6). A second system is the coordinate system of the Laue pattern. A third is an orthonormal coordinate system in the crystal which has been assigned using crystallographic conventions (Matthies, Wenk & Vinel, 1988). The ultimate goal is to relate the coordinate system of the crystal x, y, z to that of the sample X, Y, Z. For this, Euler angles α, β, γ, as defined by Matthies *et al.* (1988), are used, which require three rotations to bring the coordinate systems to coincidence.

For the derivation of the Euler angles from the indexed diffraction pattern, we adapted the method of Wright & Adams (1992, equations 6–9) for use with zone axes [*uvw*] instead of lattice planes (*hkl*). From each pair of indexed zone axes, an orthonormal frame in the form of a 3 × 3 matrix is calculated, which gives the orientation of the Laue pattern frame relative to the crystal. The spherical coordinates φ and ρ of the same pair of zone axes define a second 3 × 3 matrix, which describes the orientation of the same orthonormal frame relative to sample coordinates. Multiplication of the two matrices yields the orientation matrix between the crystal and sample frame (Wright & Adams, 1992, equations 6–9). This procedure was carried out for all possible pairs of zone axes; the resulting Euler angles are listed in Table 2. The average of these ten sets of Euler angles is α = 191.9, β = 69.9 and γ = 138.9°. Standard deviations from the average are 0.5° for α, 0.1° for β and 0.1° for γ. From these average Euler angles that define the crystal orientation (Fig. 7), and the lattice geometry, a theoretical Laue pattern for indices *hkl* up to ten was calculated, with unit intensity for all reflections. The calculated pattern (dark spots) compares very well with the observed pattern (superposed white spots) in Fig. 4(*b*). A few observed spots without calculated equivalents have Laue indices higher than ten. The apparent intensity differences in the dark spots is an artefact of the printer.

The method is described here in some detail for one diffraction pattern. Results of a full *xy* scan, covering a large sample area, will be published later. The procedure is fairly similar to that used for identifying electron-backscattering diffraction patterns. There are, however, some important differences: experimental electron-backscattering diffraction patterns display continuous straight bands of intensity, contrary to the discrete spots in the Laue patterns. For electron-backscattering diffraction patterns, bands correspond to lattice planes (*hkl*) whereas straight lines in Laue patterns correspond to zone axes [*uvw*]. Transformations are therefore different. The 'look-up' table for electron-backscattering diffraction-pattern analysis is based on a

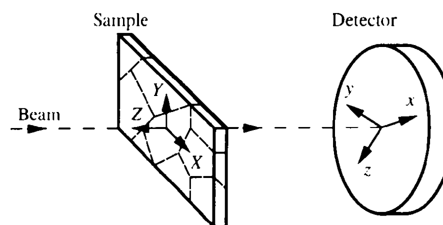

Figure 6
Schematic sketch of the polycrystalline sample with coordinate system *XYZ* and the crystal coordinate system *xyz*, the orientation of which is derived from the Laue pattern.

fairly small number of {*hkl*} families, *i.e.* between four (cubic crystal symmetry) and ten (trigonal crystal symmetry). In the present analysis we had to use about 50 families of zones ⟨*uvw*⟩ to find the correct solution. This is partly due to the low symmetry (orthorhombic), but also due to the smaller angular range of detection, which is 20–30° in this analysis as opposed to 50–60° in the analysis of electron-backscattering diffraction patterns.

4. Discussion and conclusions

A new method for automatically measuring individual orientations with synchrotron radiation has been tested and its feasibility has been established in a pilot experiment at the ESRF. An intense highly-focused beam of white X-rays probes a sample, consisting of a thin slice. In our case the beam diameter was 20–30 µm, but this could be easily reduced to 10 µm or even less. In future experiments it would be advantageous to have the sample mounted closer to the phosphor screen to obtain a larger angular range. We chose a 100 µm slice in order to have enough scattering volume. It turned out that diffracted intensities were so high that the primary beam had to be passed through an absorber. In order to reduce grain overlap it would be advantageous to have thinner samples, such as standard petrographic thin sections (30 µm) or even less. They could remain mounted on a glass slide for stability. Since the sample volumes diffract, the technique produces highly-coherent diffraction patterns and is not subject to surface damage and less affected by poor crystallinity. By using the gnomonic projection and the Hough transform, the indexing of the patterns can be fully automated, with data reduction in real time, rather than later extraction of information from huge cumbersome data arrays. Patterns can be measured and interpreted within seconds, depending on electronics and computer facilities. This is comparable with electron-backscattering diffraction-pattern analysis although electron-backscattering diffraction is more restricted to low-order reflections and therefore easier to interpret. With all procedures optimized, several samples can be measured during a 24 h run. The technique of Laue patterns to measure individual orientation is another application of synchrotron X-rays for texture analysis. Previously, monochromatic radiation has been used to document variations of average microtextures in fine-grained materials (Bäckstrøm, Riekel, Abel, Lehr & Wenk, 1996).

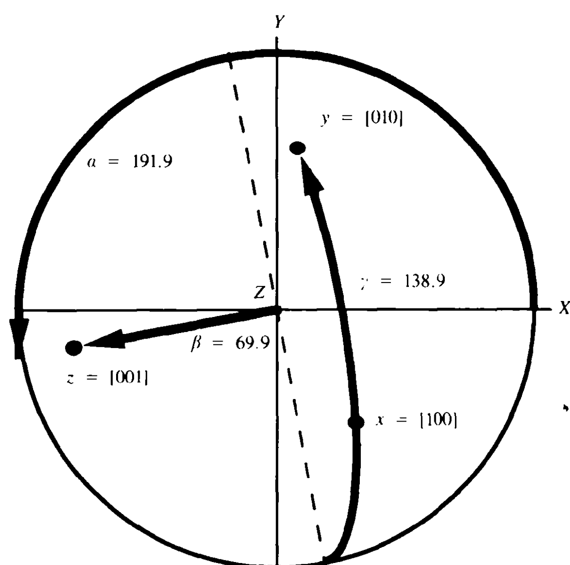

Figure 7
Stereographic projection illustrating the orientation of the olivine crystal defined by Euler angles α = 191.9, β = 69.9, γ = 138.9°.

HRW is appreciative for hospitality at CNRS during a sabbatical leave, and we are grateful for help by C. Riekel, T. Ursby and M. Wulff at the ESRF. We acknowledge helpful discussions with S. Wright, TexSEM Laboratories, about aspects of image processing. The research was supported by NSF grant EAR 94-17580.

References

Adams, B. L., Wright, S. I. & Kunze, K. (1993). *Metall. Trans.* **24**A, 819–833.
Amorós, J. L., Buerger, M. J. & Amorós, M. C. (1975). *The Laue Method.* New York: Academic Press.
Bäckstrøm, S. P., Riekel, C., Abel, S., Lehr, H. & Wenk, H. R. (1996). *J. Appl. Cryst.* **29**, 118–124.
Barrett, C. S. & Massalski, T. B. (1980). *Structure of Metals*, p. 616. Oxford: Pergamon Press.
Bunge, H. J. (1982). *Texture Analysis in Materials Science.* London: Butterworths.
Campbell, J. W., Clifton, I. J., Harding, M. M. & Hao, Q. (1995). *J. Appl. Cryst.* **28**, 635–640.
Gottstein, G. (1988). *8th International Conference on Textures of Materials*, pp. 195–202. Warrendale, USA: The Metallurgy Society.
Greenhough, T. J. & Shrive, A. K. (1994). *J. Appl. Cryst.* **27**, 111–121.
Hammersley, A. P., Svensson, S. O. & Thompson, A. (1994). *Nucl. Instrum. Methods*, A**346**, 312–321.
Helliwell, J. R., Habash, J., Cruickshank, D. W. J., Harding, M. M., Greenhough, T. J., Campbell, J. W., Clifton, I. J., Elder, M., Machin, P. A., Papiz, M. Z. & Zurek, S. (1989). *J. Appl. Cryst.* **22**, 483–497.
Hough, P. V. C. (1962). US Patent 3 069 654. 18 December.
Jacobson, R. A. (1986). *J. Appl. Cryst.* **19**, 283–286.
Krieger-Lassen, N. C., Juul Jensen, D. & Conradsen, K. (1992). *Scanning Microsc.* **6**, 115–121.
Kunze, K., Adams, B. L., Heidelbach, F. & Wenk, H. R. (1994). *Mater. Sci. Forum*, **157–162**, 1243–1249.
Kunze, K., Wright, S. I., Adams, B. L. & Dingley, D. J. (1993). *Textures Microstruct.* **20**, 41–54.
Laugier, J. & Filhol, A. (1983). *J. Appl. Cryst.* **16**, 281–283.
Matthies, S., Wenk, H. R. & Vinel, G. W. (1988). *J. Appl. Cryst.* **21**, 285–304.
Moy, J. P. (1994). *Nucl. Instrum. Methods*, A**348**, 641–644.
Sander, B. (1950). *Einführung in die Gefügekunde der Geologischen Körper*, Vol. 2, p. 194. Vienna: Springer-Verlag.
Stock, S. R., Guvenilir, A., Piotrowski, D. P. & Rek, Z. U. (1995). *Synchrotron Rad. News*, **8**, 24–25.
Wassermann, G. & Grewen, J. (1962). *Texturen Metallischer Werkstoffe.* Berlin: Springer-Verlag.

Wenk, H. R. (1985). *Preferred Orientation in Deformed Metals and Rocks: an Introduction to Modern Texture Analysis*. Orlando, FL: Academic Press.

Wenk, H. R. & Trommsdorff, V. (1965). *Beitr. Mineral. Petrogr.* **11**, 559–585.

Wright, S. I. & Adams, B. L. (1992). *Metall. Trans.* A**23**, 759–767.